Sheffield Hallam University

Atom Probe Tomography Investigation of Clustering in Model P2O5-Doped Borosilicate Glasses for Nuclear Waste Vitrification

KLUPS, P, SKERRATT-LOVE, Katrina, KRUGER, Albert, GEORGE, Jaime, BELL, Anthony <http://orcid.org/0000-0001-5038-5621>, BINGHAM, Paul <http://orcid.org/0000-0001-6017-0798>, MOODY, M and BAGOT, Paul

Available from Sheffield Hallam University Research Archive (SHURA) at:

http://shura.shu.ac.uk/33856/

This document is the author deposited version. You are advised to consult the publisher's version if you wish to cite from it.

Published version

KLUPS, P, SKERRATT-LOVE, Katrina, KRUGER, Albert, GEORGE, Jaime, BELL, Anthony, BINGHAM, Paul, MOODY, M and BAGOT, Paul (2024). Atom Probe Tomography Investigation of Clustering in Model P2O5-Doped Borosilicate Glasses for Nuclear Waste Vitrification. Microscopy and Microanalysis.

Copyright and re-use policy

See http://shura.shu.ac.uk/information.html

Sheffield Hallam University Research Archive
http://shura.shu.ac.uk

Atom Probe Tomography Investigation of Clustering in Model P2O5-Doped Borosilicate Glasses for Nuclear Waste Vitrification

Przemyslaw Klup, Katrina Skerratt-Love, Albert A Kruger, Jaime George, Anthony Martin Thomas Bell, Paul A Bingham, Michael P Moody, Paul A J Bagot

DECTRIS

ARINA with NOVENA

Fast 4D STEM

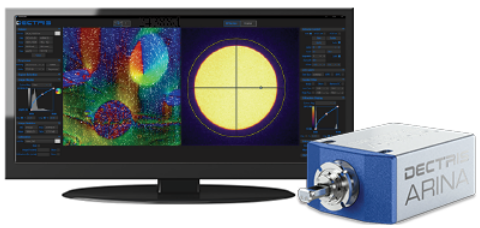

DECTRIS NOVENA and CoM analysis of a magnetic sample.

Sample courtesy: Dr. Christian Liebscher, Max-Planck-Institut für Eisenforschung GmbH.
Experiment courtesy: Dr. Mingjian Wu and Dr. Philipp Pelz, Friedrich-Alexander-Universität, Erlangen-Nürnberg.

Downloaded from https://academic.oup.com/mam/advance-article/doi/10.1093/mam/ozae059/7708979 by Sheffield Hallam University user on 15 July 2024

Microscopy and Microanalysis, 2024, **00**, 1–8
https://doi.org/10.1093/mam/ozae059

Original Article

Microscopy AND Microanalysis

Atom Probe Tomography Investigation of Clustering in Model P_2O_5-Doped Borosilicate Glasses for Nuclear Waste Vitrification

Przemyslaw Kluṕ[1], Katrina Skerratt-Love[2], Albert A. Kruger[3], Jaime George[4], Anthony Martin Thomas Bell[2], Paul A. Bingham[2], Michael P. Moody[1], and Paul A.J. Bagot[1,*]

[1]*Department of Materials, University of Oxford, Parks Road, Oxford OX1 3PH, UK*
[2]*Materials and Engineering Research Institute, Sheffield Hallam University, Sheffield S1 1WB, UK*
[3]*Office of River Protection 2440 Stevens Center Pl, Richland, WA 99354, USA*
[4]*Pacific Northwest National Laboratory, PO Box 999, Richland, WA 99352, USA*

***Corresponding author:** Paul A.J. Bagot, E-mail: paul.bagot@materials.ox.ac.uk

Abstract

Atom probe tomography (APT) has been utilized to investigate the microstructure of two model borosilicate glasses designed to understand the solubility limits of phosphorous pentoxide (P_2O_5). This component is found in certain high-level radioactive defence wastes destined for vitrification, where phase separation can potentially lead to a number of issues relating to the processing of the glass and its long-term chemical and structural stability. The development of suitable focused ion beam (FIB)-preparation routes and APT analysis conditions were initially determined for the model glasses, before examining their detailed microstructures. In a 3.0 mol% P_2O_5-doped glass, both visual inspection and sensitive statistical analysis of the APT data show homogeneous microstructures, while raising the content to 4.0 mol% initiates the formation of phosphorus-enriched nanoscale precipitates. This study confirms the expected inhomogeneities and phase separation of these glasses and offers routes to characterizing these at near-atomic scale resolution using APT.

Key words: atom, borosilicate glass, probe, tomography, vitrified waste

Introduction

Phosphorus pentoxide (P_2O_5) has been identified as a potentially problematic component of certain radioactive defence wastes arising as a result of pre-processing, such as those processed at the Hanford Site in Washington State, USA (Goel et al., 2019). In an effort to safely dispose of the waste, vitrification implementing a borosilicate glass composition is used; however, P_2O_5 is poorly soluble in borosilicate glass systems, with low concentrations potentially leading to phase separation, where this can affect key properties such as the melt viscosity and chemical durability (Schuller et al., 2008).

Understanding the detailed nature of such processes, and the solubility limits, requires high-resolution microstructural characterization methods. Atom probe tomography (APT) is a uniquely powerful technique to explore the detailed near-atomic scale microstructures of materials in 3D. While it continues to be an invaluable tool for exploring phase separation and related features in a wide range of metallic alloys, the fragile, poorly conducting nature of nonmetallic glasses makes them more challenging materials to both prepare specimens by focussed ion beam (FIB) methods and to successfully characterize them by APT. Nevertheless, the use of APT for the microstructural characterization of glasses was proposed and first demonstrated in principle over 40 years ago (Kellogg, 1982). More recently, instrumental advances have enabled researchers to make considerable progress, demonstrating feasibility for Li-doped silicate and borate glasses (Greiwe et al., 2014), transparent gahnite glass-ceramics (Mitchell et al., 2021), phosphorus and boron-doped nanocrystals within borosilicate glass (Nomoto et al., 2016), and even irradiated, hydrated borosilicate glasses (Gin et al., 2013, 2017).

In this study, our goal is to build on these earlier works, and specifically to understand how APT can be utilized to characterize two model glass materials with different P_2O_5-doping levels, based on the more chemically complex Hanford radioactive glasses (Dixon et al., 2019). With these, we aim to assess the overall suitability of APT to examine such glasses and its potential to complement existing techniques on the same samples (Skerratt-Love et al., 2023), along with exploring the early stages of phase separation to inform mechanistic understanding.

Experimental Methods

Two glass samples, labeled NBSP3.0 and NBSP4.0 with differing amounts of P_2O_5 were examined. The nominal compositions of these samples (in mol%) were: 54.14 SiO_2–15.79 B_2O_3–3.0 P_2O_5–27.07 Na_2O (NBSP3.0) and 53.58 SiO_2–15.63 B_2O_3–4.00 P_2O_5–26.79 Na_2O (NBSP4.0) (Skerratt-Love et al., 2023). The compositions of these samples were verified (using XRF and ICP-OES) by Skerratt-Love et al. (2023).

Samples for APT were prepared using a Ga^+ ion SEM-FIB (Zeiss Crossbeam 550) following the standard lift-out protocol (Miller et al., 2005). The borosilicate glass material proved

Received: November 30, 2023. **Revised:** May 27, 2024. **Accepted:** June 18, 2024
© The Author(s) 2024. Published by Oxford University Press on behalf of the Microscopy Society of America.
This is an Open Access article distributed under the terms of the Creative Commons Attribution License (https://creativecommons.org/licenses/by/4.0/), which permits unrestricted reuse, distribution, and reproduction in any medium, provided the original work is properly cited.

Downloaded from https://academic.oup.com/mam/advance-article/doi/10.1093/mam/ozae059/7708979 by Sheffield Hallam University user on 15 July 2024

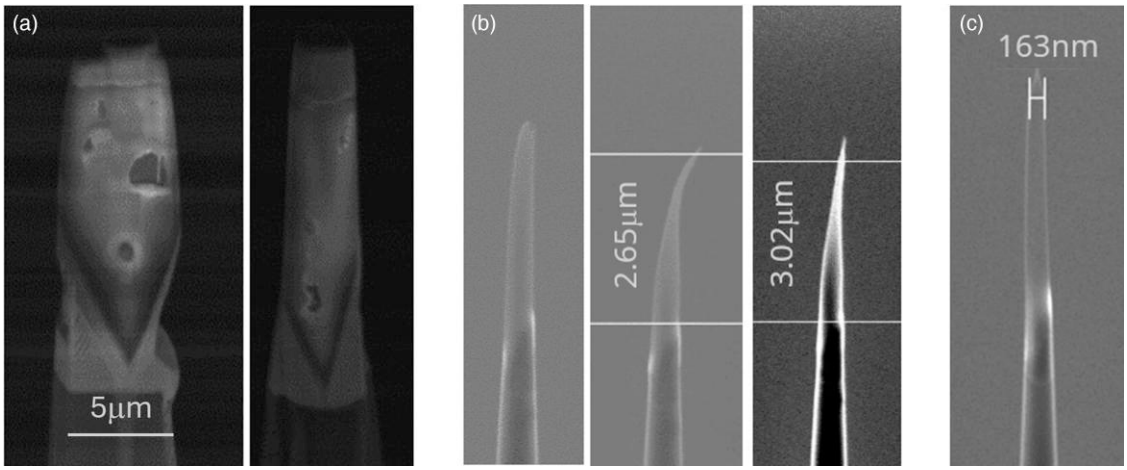

Fig. 1. (**a**) FIB preparation on mounted lift-out wedges of borosilicate glass on Si coupon, showing regions of porosity present. (**b**) Early attempts at final specimen sharpening showed the bending of tip apexes (2 nA e-beam current). (**c**) Revised sharpening protocol (0.5 nA) demonstrating viable specimen production.

relatively straightforward to work with in the FIB, aside from encountering occasional regions of low density/pores in the lift-out volumes (Fig. 1a). However, an issue was noted in the final stage of specimen sharpening, where for apex radii less than 200 nm, SEM imaging appeared to induce a bending deflection in the tips. This is shown in three examples in Figure 1b. In some cases, these could be straightened by further polishing (at 2 kV: 200 pA), but often such deflections resulted in nonviable final specimens. A very similar issue was encountered in a recent study of Sr-doped bioglass for bone scaffolding applications (Ren et al., 2021), which was attributed to excessive electron beam heating. Lowering the SEM beam current from 2 to 0.5 nA prevented this issue from recurring, as demonstrated in Figure 1c, underlining the general advice to minimize electron beam currents (and doses).

Viable samples were all subsequently analyzed in a Cameca LEAP 5000 XR (Oxford University). Following a short study of the influence of the analysis conditions on the data quality, all specimens examined in depth were run using a stage temperature of 45 K, laser pulse energy of 200 pJ, pulsing frequency of 200 kHz, and a target evaporation rate of 0.2%. In total, 16 datasets were obtained across the study, from which 10 were deemed suitable for quantitative interpretation (sufficient number of ions (>3 M), low background noise (<80 ppm/ns), well-resolved mass spectra peaks). All datasets were reconstructed and analyzed using IVAS 3.8.16, with later preparation of correlation histograms carried out using the in-built algorithms within AP Suite 6.3.

Results

Reconstruction Optimization

In general, all viable-looking specimens from the FIB preparation ran satisfactorily in the LEAP, with datasets larger than 20 M ions routinely obtained. Neither changes to the stage temperature (35–55 K), nor the laser pulse energy (lowering to 150 pJ) had any measurable positive impact on the data, with reductions in the latter causing the signal-to-noise ratio to deteriorate. The level of multiple hits was within a reasonable range for nonmetallic materials, typically 25–35%. However, the voltage evolution fluctuated throughout each experiment, indicative perhaps of the influence of the very low electrical conductivity of borosilicate glass (10^{-11}–10^{-13} S/m) on the evaporation of the specimen (Boccaccini et al., 2007). This ruled out reconstructing the apex shape using a conventional voltage-evolution approach, further complicating the data reconstruction on top of having a multi-component system with unknown evaporation field(s). To make progress and standardize the reconstructions so that they could be directly compared with each other, a density-based approach was used at the initial reconstruction stage, making use of the nominal borosilicate glass density of 2.2 g/cm^3 (which for LEAP 5000 XR systems with detection efficiency of 52% is equivalent to 0.085 atoms/nm^3). Reconstructions were also based around a fixed-shank profile.

Bulk Composition

Figure 2 shows a typical mass spectrum, in this case from the NBSP4.0 material. A complex pattern of peaks is apparent, with elemental and molecular oxygen-containing ions detected across the full spectrum. The mass resolution is sufficiently high to enable clear identification of most peaks, and while there is some evidence of delayed evaporation post-laser pulse (higher background level following some peaks, $^{23}Na^+$ in particular), the extent of this does not preclude identification of the following minor peaks. Due to the number of complex ions evaporated and fragmenting *en route* to the detector, some peak overlaps are present. By inspection of the spatial location of ions in other similar peaks, e.g., PO_2 and PO, along with careful use of IVAS's peak decomposition algorithm, it was however possible to assign the majority of peaks with a reasonable degree of confidence. There was negligible sign of any unexpected contaminant elements in all samples examined.

Table 1 shows the determined compositions of both glasses, shown as (mean) values averaged across all equivalent datasets, along with nominal values. Note the nominal values shown here (in at%) are equivalent to those given (in mol%) introduced above, which are retained for easy comparison with the existing companion study on these glasses (Skerratt-Love et al., 2023). Acceptably close agreement is apparent for nearly all elements. The Na is somewhat lower than expected while the P content is higher, although in the latter the APT data does track the trend in this rising from NBSP3.0 to NBSP4.0.

Downloaded from https://academic.oup.com/mam/advance-article/doi/10.1093/mam/ozae059/7708979 by Sheffield Hallam University user on 15 July 2024

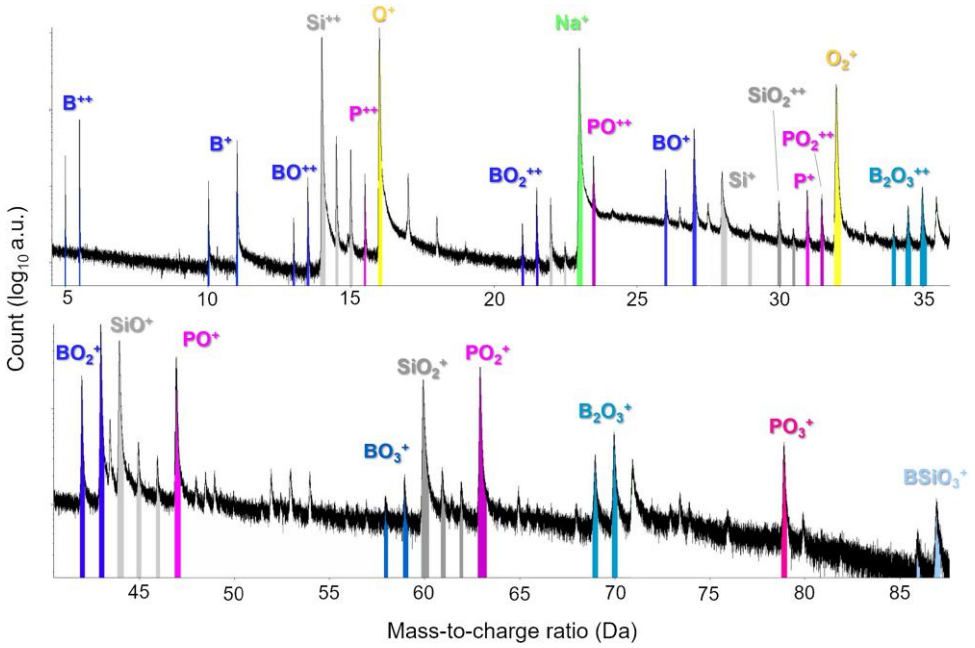

Fig. 2. Example mass spectrum (split into low and high mass-to-charge ratios) from NBSP4.0. Recorded on LEAP 5000XR at 45 K, 200 pJ pulse energy, and 200 kHz pulsing frequency.

While the spectra return accurate compositions, it is also apparent from Figure 2 that there is a relatively high level of noise present, particularly following the major peaks. This is indicative of delayed evaporation of ions appearing later than those within the main peaks, and examining correlations between such ions can provide deeper insights into the field evaporation behavior. In practice, this is made possible by the use of correlation histograms (Saxey, 2011), which plot correlations between pairs of ions evaporating as multi-ion events. The frequency of such ion-pair coincidences (P_{ij}) for ion types i and j can be compared with that expected from a completely random distribution to determine any statistically significant correlations for every ion pair. Figure 3 shows an example of these, generated from a NBSP4.0 dataset. This plots multiple ion events detected up to 50 Da on both axes. To interpret these, note the sets of vertical, horizontal, and diagonal lines, originating from a point corresponding to the detection of an ion at a specific mass-to-charge-state ratio. The first two sets of lines correspond to field evaporation of ion type i (or equivalently j) on the applied laser pulse, followed some short time after the pulse by evaporation of the paired ion j. The diagonal lines running toward the top-right corner, therefore, show co-evaporation of ions i and j both at some time delay after the pulse. The intensity of these diagonal tracks originating from any point are reflective of the magnitude of the tail apparent in the conventional mass spectrum, and it is apparent that the most dominant tracks all run along the $y = x$ line, which marks evaporation of ions of the same type (i.e., ion type $i = j$). In terms of the field evaporation behavior of the borosilicate glass, this plot reveals a number of details. Firstly, the strength and extent of the diagonal lines, tracking away from their origins across a large extent of the plot, signifies many ions evaporating at times after the initial pulse. The strongest intensity of track originates at 23 Da, ranged as Na^+, which correlates to the significant tail in this peak observed in the mass spectrum of Figure 2 extending all the way up to the next major peak at 32 Da (O_2^+). The length of all such tracks is indicative of the evaporation behavior of a material with (as known) low thermal conductivity.

Away from the major diagonal, there are a considerable number of tracks again with lengthy tails, signifying (delayed) evaporation of dissimilar ions. Some of these are marked by dotted circles in Figure 3. (For brevity, only selected (i, j) pairs below the main $y = x$ diagonal are discussed below, but note the equivalent (j, i) ions are also circled in Figure 3 with the same color). The green circle (16, 23 Da) corresponds to (O^+, Na^+), likely indicative of the post-fragmentation of the Na_2O glass component. The gray circle (43, 32 Da) shows (SiO^+, O_2^+), and finally, the pink circle (63, 43 Da) reveals paired evaporation for (PO_2^+, BO_2^+). Such events point to fragmentation of the constituent glass components. This suggests that a higher standing field (i.e., lower laser pulse power) during specimen analysis might be desirable to break up such large ions, however, on the current set of samples attempts to do this resulted in premature specimen fracture, underlining the compromises which must be made for challenging materials. Collectively, these plots underline the complex nature of ions evaporating from the borosilicate, with many pairs of ions evaporating off-pulse. This is also reflected by the relatively high level of multiple hits noted in these experiments, and indeed the high background noise level within the mass spectra; efforts to reduce this to around 100 ppm/ns improved the signal-to-noise, but this is still high compared with metals for example, where ~10 ppm/ns is more common. We stress however that despite the complex evaporation behavior, the peak overlap decomposition (identification) tools are able to return accurate compositions.

Microstructural Details

In many specimens from both sample materials, fluctuating levels of Na were apparent. It is well known that in certain materials that recorded positions of Na atoms may be influenced by surface diffusion prior to field evaporation, impairing

Downloaded from https://academic.oup.com/mam/advance-article/doi/10.1093/mam/ozae059/7708979 by Sheffield Hallam University user on 15 July 2024

Table 1. APT Compositional Data From NBSP3.0 and NBSP4.0, Averaged Over Multiple Runs (Errors Report Standard Deviation Across Set of Experiments), Compared With Nominal.

	O	Si	Na	B	P
NBSP3.0—at%					
Nominal	55.5	18.2	18.0	7.9	0.9
APT	54.3 ± 0.4	19.5 ± 0.6	15.7 ± 0.8	8.25 ± 0.77	2.31 ± 0.42
NBSP4.0—at%					
Nominal	55.3	17.9	17.9	7.8	1.1
APT	55.5 ± 0.3	17.6 ± 0.2	13.2 ± 0.9	9.73 ± 0.35	3.96 ± 0.20

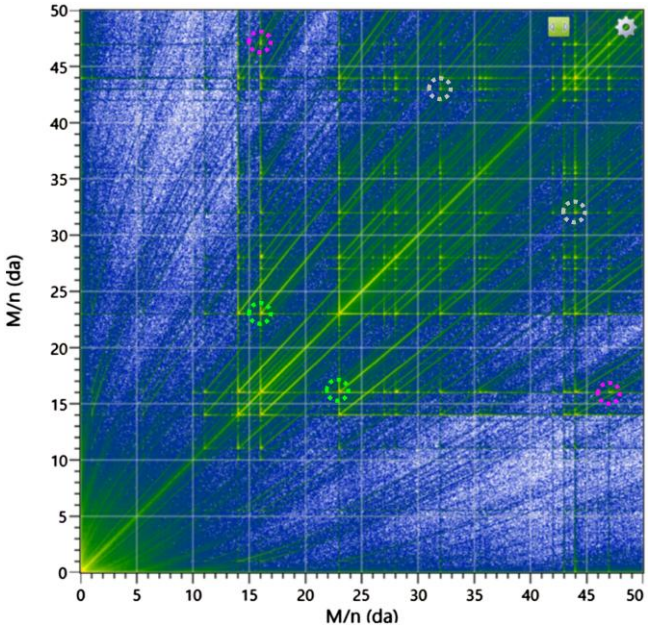

Fig. 3. Correlation histogram for NBSP4.0 borosilicate glass, analyzed in a LEAP 5000XR at 45 K, 200 pJ pulse energy, and 200 kHz pulse frequency. Double and triple multiple hits shown across 0–50 Da. For an explanation of dotted circles and tracks, refer to the main text.

accurate reconstruction (Miller et al., 1996; Li et al., 2014). The regular bursts of Na noted in the detector hit maps, along with the extent of the tracks in the correlation histogram are both consistent with its relatively low theoretical evaporation field compared with those known for other glass components (11 V/nm for Na^+ versus 33 V/nm for Si^+) which flags the likelihood of any Na-rich phases being most likely related to artifacts. Additionally, there are no mentions of such phases found using other techniques in a complementary study of these same glasses (Skerratt-Love et al., 2023). Therefore, while we show the Na spatial distributions in the following datasets for full disclosure, in the current work we assume Na fluctuations are an artifact, and are consequently not examined in depth.

Figure 4a is an atom map from sample NBSP3.0 showing all main elemental components, with a fraction of each ion type magnified. This visually illustrates a homogeneous volume, confirmed by the 1D concentration profile in Figure 4b (same scale), running along the main *z*-axis of the reconstruction (minor Na fluctuations aside). To examine in particular the P-distributions in more detail, a more sensitive statistical test of any inhomogeneities is given by a nearest neighbor analysis, which is shown for $P(O_x)$ in Figure 4c. The black dotted line corresponds to the expected nearest neighbor distribution in a fully homogeneous material, while the magenta line shows the actual distributions measured. The two lines closely overlap, indicating the $P(O_x)$ distribution is very close to that of random one, and with no evidence of any secondary precipitation of a P-rich phase in the 3.0 mol% P_2O_5 sample, NBSP3.0.

Figures 5a to 5c show the corresponding atom map, 1D concentration profile, and nearest neighbor distribution for NBSP4.0. The atom maps display B/BO_x species, along with an isoconcentration surface (isosurface) set at 8.8 at% P. In this figure, we also show a 30 at% Na isosurface, to illustrate the nature of the Na segregation artifact as flattened discs all arranged perpendicular to the analysis direction (coinciding with evaporation bursts). Of more interest however, this map shows that the glass now contains localized regions enriched in P throughout. These have an approximately spherical structure in a number of instances, around 20 nm in diameter. Although these reconstructed volumes are potentially distorted due to the erratic nature of the evaporation, similarly shaped structures have been identified in high-resolution SEM, thus the APT data is likely showing morphologies of these as they nucleate and grow. The 1D concentration profile in Figure 5b also captures the inhomogeneous microstructure, with Si, O (and Na) levels fluctuating significantly. Finally, Figure 5c statistically examines the $P(O_x)$ distribution, clearly verifying the nonrandom P-rich segregation behavior, demonstrating that a small increase in the P_2O_5 loading has initiated phase separation in the NBSP4.0 glass.

Figure 6 presents a more detailed examination of the precipitation, focussing on one section from a NBSP4.0 analysis. Figures 6a and 6b (400 nm long in depth) show atom two maps breaking down the ions into O, B (Fig. 6a) and Na, Si (Fig. 6b) species, in both cases with the same (7.5 at%) P isoconcentration surface. The distribution of precipitates highlighted by the isoconcentration surface is nonuniform, perhaps indicative of nucleation on defects within the glass microstructure, with clusters of P-rich phases located within 10 nm of each other. Figure 6c displays a proxigram averaged across all combined common interfaces in the shown atom maps. These facilitate the examination of both the volume fraction and composition of the P-rich phases. The volume fraction was estimated by dividing all (ranged) atoms contained within one set of surfaces by the total number of (ranged) atoms in the dataset, which returns an average value of 2.7%. The measured composition (at%) of the precipitates is 58.1 O–15.0 Na–13.5 P–8.2 Si–5.2 B. This is somewhat different from the expected formation of either Na_3PO_4 or $Na_4P_2O_7$, although the nominal oxygen (50 at%) and phosphorous (13 at%) contents are quite close to the former, with a loss of sodium and unexpected Si and B. The lower Na content may be a result of Na diffusion to co-located Na regions during the field evaporation process; although not

Downloaded from https://academic.oup.com/mam/advance-article/doi/10.1093/mam/ozae059/7708979 by Sheffield Hallam University user on 15 July 2024

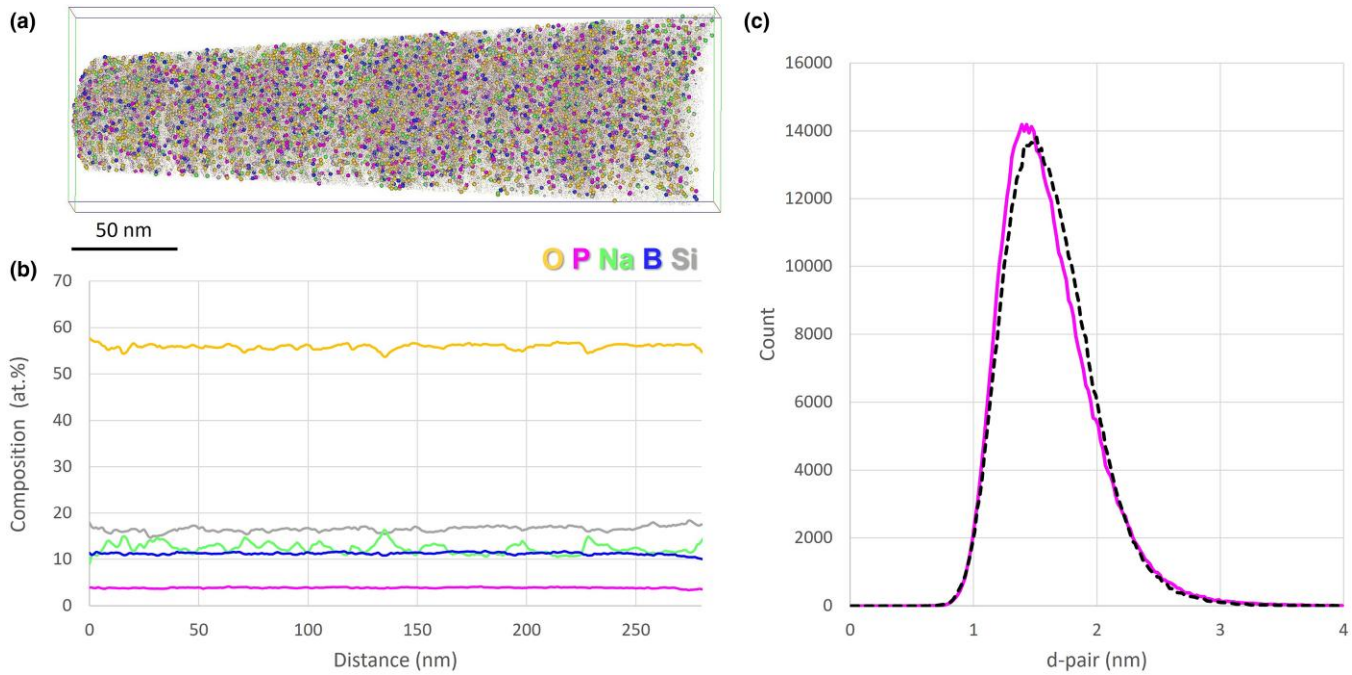

Fig. 4. (**a**) Atom map of sample NBSP3.0 and (**b**) corresponding 1D concentration profile (same scale), demonstrating uniformity of composition throughout. 10% of selected species are shown as larger spheres in (**a**) for visual clarity. (**c**) Nearest neighbor statistical analyses for $P(O_x)$ species, comparing experimental data (solid magenta line) with randomized reference (dotted black line). Close fit verifies homogeneous microstructure.

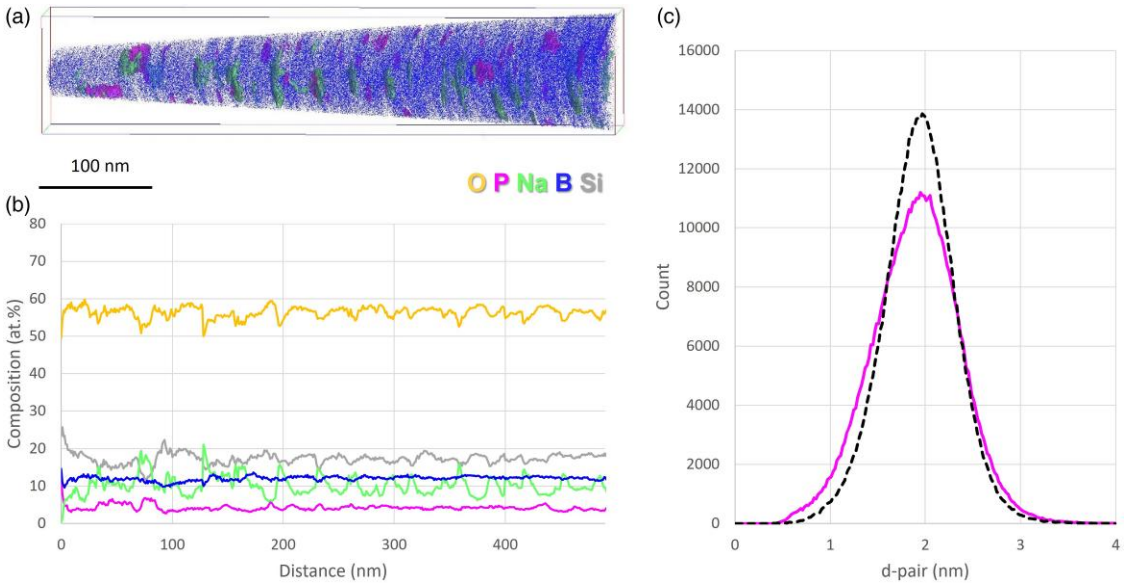

Fig. 5. (**a**) Atom map of sample NBSP4.0 with B/BO_x species shown (blue dots), along with 8.8 at% P (and 30 at% Na) isoconcentration surfaces highlighting phase separation. (**b**) Corresponding 1D concentration profile (same scale), showing composition fluctuations, mostly strikingly for Na, Si and O. (**c**) Nearest neighbor statistical analyses for $P(O_x)$ species, comparing experimental data (solid magenta line) with fully randomized reference (dotted black line).

examined in depth these features (as shown in Fig. 5) consistently contained more than 50 at% Na.

Discussion

A primary goal in the current work was to determine whether these simplified, surrogate radioactive waste-form borosilicate glasses were amenable to APT characterization. The results herein demonstrate that it is possible to generate reproducible datasets, and that the returned compositions are closely in-line with expectations. However, it is also apparent that the material is evaporating in a somewhat nonuniform manner, complicating efforts to reconstruct the data. Additional experiments were carried out to examine the role of laser pulse frequency on the data quality, examining the background noise level and voltage profile while the pulse frequency was varied

Downloaded from https://academic.oup.com/mam/advance-article/doi/10.1093/mam/ozae059/7708979 by Sheffield Hallam University user on 15 July 2024

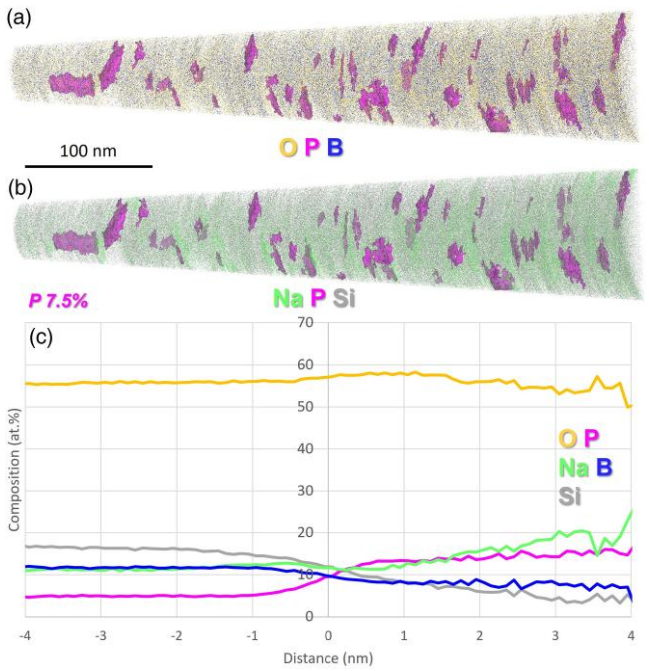

Fig. 6. (**a, b**) Atom maps from NBSP4.0 specimens (400 nm in depth) with 7.5 at% P isoconcentration surfaces (pink) highlighting phase separation. (**c**) Proxigram taken from across the respective interfaces shown in (**a, b**). Core volumes within these proxigrams (right-hand side) show the formation of possible Na_3PO_4/$Na_4P_2O_7$-type phases.

from 25, 50, 100, and then 200 kHz. There did not however to appear to be any real correlation of these metrics with pulse frequency, although attempts to analyze specimens at higher frequency (250 and 500 kHz) resulted in rapid fracture. Higher frequency also coincided with more Na-rich phases, while at lower frequencies they disappeared which further supports the argument the formation of these regions is an APT artifact. Higher laser pulse frequencies can cause both off-pulse evaporation and a higher failure probability, which reinforces the idea that some of the supplied laser thermal energy is being retained between pulses within the specimen apex. Thermal energy from the laser is also likely contributing to the surface diffusion of Na species to localized regions returning unexpectedly high sodium contents; in a similar manner, overly high laser pulse energies have also been seen to cause surface diffusion of boron atoms in silicon (Tu et al., 2017). The retention of heat in this material and its effect on field evaporation behavior in the APT is also highlighted by the intense and extended post-pulse tracks shown in correlation histogram of Figure 3.

Similar effects of laser irradiation on these types of glasses have been previously demonstrated in the work of Lu et al. (2017), who showed that APT mass spectra measured in the analysis of a model International Simple Glass (ISG) consisting of six oxides, and that from a more complex French-grade SON68 glass, were both prone to the effects of delayed field evaporation when utilizing a 532 nm laser. The 355 nm beam on the LEAP 5000 system yielded sharper mass spectra, although still with a complex number of peaks present and with locally high background levels.

Nomoto et al. (2016) presented a series of APT mass spectra from boron or phosphorous-doped silicon nanocrystals embedded in borosilicate, phosphosilicate, and borophosphosilicate glasses, as examined in a LEAP 4000Si system with a laser pulse energy of 100 pJ. All of these illustrated substantial thermal tails throughout the mass spectra, yet this did not prevent the characterization of distinct Si, B, and P-rich nanoclusters present in the datasets. Gin et al. (2013) examined the French-grade SON68 glass, with a more complex composition containing Al, B, Ca, Li, Na, O, and Si, along with trace (<1 at%) Fe, Mo, and Zr. As-received and hydrated forms of this were examined in a Cameca LEAP 4000XHR. Comparable analysis conditions were used in this work (aside from lower laser pulse energies), with the authors similarly reporting no significant differences in chemical or spatial information when altering them. A slight loss of oxygen was apparent and attributed to the known issue of preferential oxygen loss through formation of neutral, undetected atoms/molecules, as seen in a wide range of oxygen-containing materials (Devaraj et al., 2013; Amirifar et al., 2015; Karahka et al., 2015; Santhanagopalan et al., 2015; Cappelli et al., 2021). The oxygen content in the current study does not appear to be significantly affected by such a mechanism. However, differences in composition through the hydration exposure in this earlier work were accurately reflected in the comparative analyses, which is also true here for the increase in P_2O_5 loading. Spatial reconstructions of the APT data were carried out with the aid of SEM images of the tip shape, while in a later study by Gin et al. (2017) on a standard 6-oxide borosilicate glass, fixed-shank angles were used to reconstruct the datasets, which is also apparent in the work on a corroded SON68 borosilicate glass of Perea et al. (2020). The use of these reconstruction approaches suggests some uncertainty in the known evaporation behavior of these glasses, although this does not prevent high-quality compositional data being obtained. Perea et al. (2020) explore the use of cryogenic conditions to prepare their specimens in FIB, and this approach does appear to smooth the evolution of the voltage curve through a glass-gel interface in particular. This indicates advanced sample preparation strategies, also including the possible use of conductive coatings (Adineh et al., 2017), may further improve the data quality in such glasses.

A second goal was to examine the potential for phase separation in this glass on raising the P_2O_5 content introduced during processing. The APT data shows clearly in visual and statistical analyses that the 3 mol% P_2O_5 sample has a homogeneous microstructure, while increasing the P_2O_5 loading to 4 mol% results in the formation of a new phase (excluding the Na-rich artifact) in the parent glass. This is present as finely distributed, nanoscale precipitates, collectively comprising a few percent volume fraction of the glass. The exact shape of these is uncertain due to reconstruction artifacts; however, its composition is comparable to most likely the Na_3PO_4 or $Na_4P_2O_7$ expected phases. Importantly, the findings from this work are also in excellent agreement with those obtained from a companion study on the same materials, with phase separation occurring in samples with ≥4 mol% P_2O_5, as seen using SEM and XRD (Skerratt-Love et al., 2023). Although a range of analysis conditions were explored to further improve the reconstructions, it is clear that this and related glasses do retain challenges in terms of their response to the laser pulsing conditions. These challenges include the uneven evaporation behavior, on top of the separate issue of high Na mobility and the influence of laser pulse energy on its spatial distribution and quantification. This may be further improved on newer LEAP 6000 systems, utilizing even shorter

Downloaded from https://academic.oup.com/mam/advance-article/doi/10.1093/mam/ozae059/7708979 by Sheffield Hallam University user on 15 July 2024

laser wavelengths, as these have been seen in prior instrument evolutions to greatly improve sample viability. Despite requiring further work to improve overall data quality, it is clear that APT can offer considerable insights into the microstructure of borosilicate glasses, informing design and processing steps to produce optimal materials for safer and predictable nuclear waste vitrification.

Conclusions

This study has shown that in two borosilicate glasses, respectively doped with differing levels of P_2O_5, unique characterization insights in the resulting microstructures can be provided by APT. Specifically, we have shown that:

- Both forms of borosilicate glass can be routinely and reliably characterized using LEAP 5000 instruments. Quantitative compositional information can be extracted, and physically accurate reconstructions based on known material density can be obtained.
- Na-rich regions when detected are most likely an APT artifact due to surface migration caused by a significantly lower relative evaporation field of Na. The presence of such regions can be diminished by using lower laser pulse frequencies.
- The 3 mol% P_2O_5-containing glass demonstrates a uniform, homogeneous microstructure.
- The 4 mol% P_2O_5-containing glass, in contrast, shows clear nucleation of a probable (sodium-depleted) Na_3PO_4 or $Na_4P_2O_7$ phase.
- The phase separation trends are consistent with known limits for the vitrified retention of P_2O_5-containing nuclear wastes, informing material selection by near-atomic scale characterization of such glasses.

Availability of Data and Materials

The authors have declared that no datasets apply for this piece.

Acknowledgments

The LEAP 5000 XR facility was funded by EPRSC's National Nuclear User Facility grant (EP/T011505/1), along with providing K.S.-L. with funded user access for experimental work. P.K. is supported by a Rolls-Royce studentship. The authors would like to acknowledge the help of Dr Yanru Ren, Dr James O. Douglas, and Ruiying Shu in exploring the optimal parameters for FIB preparation as well as APT experiments. Funding from K.S.-L., A.A.K., A.M.T.B., and P.A.B. is acknowledged by Sheffield Hallam University (SHU) and the US Department of Energy Office of River Protection (ORP).

Financial Support

The current study hasn't received any fund from any organizations or institutions.

Conflict of Interest

The authors declare that they have no competing interest.

References

Adineh VR, Marceau RKW, Chen Y, Si KJ, Velkov T, Cheng W, Li J, Fu J (2017). Pulsed-voltage atom probe tomography of low conductivity and insulator materials by application of ultrathin metallic coating on nanoscale specimen geometry. *Ultramicroscopy* **181**, 150–159. https://doi.org/10.1016/j.ultramic.2017.05.002

Amirifar N, Lardé R, Talbot E, Pareige P, Rigutti L, Mancini L, Houard J, Castro C, Sallet V, Zehani E, Hassani S, Sartel C, Ziani A, Portier X (2015). Quantitative analysis of doped/undoped ZnO nanomaterials using laser assisted atom probe tomography: Influence of the analysis parameters. *J Appl Phys* **118**(21), 215703. https://doi.org/10.1063/1.4936167

Boccaccini AR, Thomas BJC, Brusatin G & Colombo P (2007). Mechanical and electrical properties of hot-pressed borosilicate glass matrix composites containing multi-wall carbon nanotubes. *J Mater Sci* **42**(6), 2030–2036. https://doi.org/10.1007/s10853-006-0540-7

Cappelli C, Smart S, Stowell H & Pérez-Huerta A (2021). Exploring biases in atom probe tomography compositional analysis of minerals. *Geostand Geoanalytical Res* **45**(3), 457–476. https://doi.org/10.1111/ggr.12395

Devaraj A, Colby R, Hess WP, Perea DE & Thevuthasan S (2013). Role of photoexcitation and field ionization in the measurement of accurate oxide stoichiometry by laser-assisted atom probe tomography. *J Phys Chem Lett* **4**(6), 993–998. https://doi.org/10.1021/jz400015 h

Dixon D, Stewart C, Venarsky J, Peterson J, Hall G, Levitskaia T, Allred J, Eaton W, Lang J, Hall M, Cutforth D, Rovira A, Peterson R (2019). Vitrification of Hanford tank waste 241-AP-107 in a continuous laboratory-scale melter. *PNNL* **28361**, 1505629. https://doi.org/10.2172/1505629

Gin S, Jollivet P, Barba Rossa G, Tribet M, Mougnaud S, Collin M, Fournier M, Cadel E, Cabie M, Dupuy L (2017). Atom-probe tomography, TEM and ToF-SIMS study of borosilicate glass alteration rim: A multiscale approach to investigating rate-limiting mechanisms. *Geochim Cosmochim Acta* **202**, 57–76. https://doi.org/10.1016/j.gca.2016.12.029

Gin S, Ryan JV, Schreiber DK, Neeway J & Cabié M (2013). Contribution of atom-probe tomography to a better understanding of glass alteration mechanisms: Application to a nuclear glass specimen altered 25 years in a granitic environment. *Chem Geol* **349–350**, 99–109. https://doi.org/10.1016/j.chemgeo.2013.04.001

Goel A, McCloy JS, Pokorny R & Kruger AA (2019). Challenges with vitrification of Hanford high-level waste (HLW) to borosilicate glass – An overview. *J Non-Cryst Solids X* **4**, 100033. https://doi.org/10.1016/j.nocx.2019.100033

Greiwe G-H, Balogh Z & Schmitz G (2014). Atom probe tomography of lithium-doped network glasses. *Ultramicroscopy* **141**, 51–55. https://doi.org/10.1016/j.ultramic.2014.03.007

Karahka M, Xia Y & Kreuzer HJ (2015). The mystery of missing species in atom probe tomography of composite materials. *Appl Phys Lett* **107**(6), 062105. https://doi.org/10.1063/1.4928625

Kellogg GL (1982). Field ion microscopy and pulsed laser atom-probe mass spectroscopy of insulating glasses. *J Appl Phys* **53**(no. 9), 6383–6386. https://doi.org/10.1063/1.331509

Li T, Bagot PAJ, Christian E, Theobald BRC, Sharman JDB, Ozkaya D, Moody MP, Tsang SCE, Smith GDW (2014). Atomic imaging of carbon-supported Pt, Pt/Co, and Ir@Pt nanocatalysts by atom-probe tomography. *ACS Catal* **4**(2), 695–702. https://doi.org/10.1021/cs401117e

Lu X, Schreiber DK, Neeway JJ, Ryan JV & Du J (2017). Effects of optical dopants and laser wavelength on atom probe tomography analyses of borosilicate glasses. *J Am Ceram Soc* **100**(10), 4801–4815. https://doi.org/10.1111/jace.14987

Miller MK, Cerezo A, Hetherington MG & Smith GDW (1996). Atom probe field ion microscopy. In *Monographs on the Physics and Chemistry of Materials, No. 52*. New York: Clarendon Press, Oxford University Press.

Miller MK, Russell KF & Thompson GB (2005). Strategies for fabricating atom probe specimens with a dual beam FIB. *Ultramicroscopy* **102**(4), 287–298. https://doi.org/10.1016/j.ultramic.2004.10.011

Downloaded from https://academic.oup.com/mam/advance-article/doi/10.1093/mam/ozae059/7708979 by Sheffield Hallam University user on 15 July 2024

Mitchell AL, Perea DE, Wirth MG, Ryan JV, Youngman RE, Rezikyan A, Fahey AJ, Schreiber DK. (2021). Nanoscale microstructure and chemistry of transparent gahnite glass-ceramics revealed by atom probe tomography. *Scr Mater* **203**, 114110. https://doi.org/10.1016/j.scriptamat.2021.114110

Nomoto K, Sugimoto H, Breen A, Ceguerra AV, Kanno T, Ringer SP, Wurfl IP, Conibeer G, Fujii M (2016). Atom probe tomography analysis of boron and/or phosphorus distribution in doped silicon nanocrystals. *J Phys Chem C* **120**(31), 17845–17852. https://doi.org/10.1021/acs.jpcc.6b06197

Perea DE, Schreiber DK, Ryan JV, Wirth MG, Deng L, Lu X, Du J, Vienna JD (2020). Tomographic mapping of the nanoscale water-filled pore structure in corroded borosilicate glass. *npj Mater Degrad* **4**(1), 8. https://doi.org/10.1038/s41529-020-0110-5

Ren Y, Autefage H, Jones JR, Stevens MM, Bagot PAJ & Moody MP (2021). Developing atom probe tomography to characterize Sr-loaded bioactive glass for bone scaffolding. *Microsc Microanal* **28**(4), 1–11. https://doi.org/10.1017/S1431927621012976

Santhanagopalan D, Schreiber DK, Perea DE, Martens RL, Janssen Y, Khalifah P, Meng YS (2015). Effects of laser energy and wavelength on the analysis of $LiFePO_4$ using laser assisted atom probe tomography. *Ultramicroscopy* **148**, 57–66. https://doi.org/10.1016/j.ultramic.2014.09.004

Saxey DW (2011). Correlated ion analysis and the interpretation of atom probe mass spectra. *Ultramicroscopy* **111**(6), 473–479. https://doi.org/10.1016/j.ultramic.2010.11.021

Schuller S, Pinet O, Grandjean A & Blisson T (2008). Phase separation and crystallization of borosilicate glass enriched in MoO_3, P_2O_5, ZrO_2, CaO. *J Non-Cryst Solids* **354**(2–9), 296–300. https://doi.org/10.1016/j.jnoncrysol.2007.07.041

Skerratt-Love KL, George JL, Bell AMT, Sweeney F, Cutforth D, Lonergan CE, Dixon DR, Kruger AA, Bingham PA (2023). The effects of phosphorus pentoxide additions on the thermal, rheological, and structural properties of sodium borosilicate glass. *J Non-Cryst Solids* **600**, 121999. https://doi.org/10.1016/j.jnoncrysol.2022.121999

Tu Y, Takamizawa H, Han B, Shimizu Y, Inoue K, Toyama T, Yano F, Nishida A, Nagai Y (2017). Influence of laser power on atom probe tomographic analysis of boron distribution in silicon. *Ultramicroscopy* **173**, 58–63. https://doi.org/10.1016/j.ultramic.2016.11.023

Downloaded from https://academic.oup.com/mam/advance-article/doi/10.1093/mam/ozae059/7708979 by Sheffield Hallam University user on 15 July 2024